Open Archive TOULOUSE Archive Ouverte (OATAO)

OATAO is an open access repository that collects the work of Toulouse researchers and makes it freely available over the web where possible.

Any correspondence concerning this service should be sent to the repository administrator: staff-oatao@listes-diff.inp-toulouse.fr

Turbulent Fluid Acceleration Generates Clusters of Gyrotactic Microorganisms

Filippo De Lillo,[1] Massimo Cencini,[2,*] William M. Durham,[3] Michael Barry,[4]
Roman Stocker,[4] Eric Climent,[5] and Guido Boffetta[1]

[1]*Dipartimento di Fisica and INFN, Università di Torino, via P. Giuria 1, 10125 Torino, Italy*
[2]*Istituto dei Sistemi Complessi, Consiglio Nazionale delle Ricerche, via dei Taurini 19, 00185 Rome, Italy*
[3]*Department of Zoology, University of Oxford, South Parks Road, Oxford OX1 3PS, United Kingdom*
[4]*Ralph M. Parsons Laboratory, Department of Civil and Environmental Engineering, Massachusetts Institute of Technology,*
77 Massachusetts Avenue, Cambridge, Massachusetts 02139, USA
[5]*Institut de Mécanique des Fluides, Université de Toulouse, INPT-UPS-CNRS, Allée du Pr. Camille Soula, F-31400 Toulouse, France*

The motility of microorganisms is often biased by gradients in physical and chemical properties of their environment, with myriad implications on their ecology. Here we show that fluid acceleration reorients gyrotactic plankton, triggering small-scale clustering. We experimentally demonstrate this phenomenon by studying the distribution of the phytoplankton *Chlamydomonas augustae* within a rotating tank and find it to be in good agreement with a new, generalized model of gyrotaxis. When this model is implemented in a direct numerical simulation of turbulent flow, we find that fluid acceleration generates multifractal plankton clustering, with faster and more stable cells producing stronger clustering. By producing accumulations in high-vorticity regions, this process is fundamentally different from clustering by gravitational acceleration, expanding the range of mechanisms by which turbulent flows can impact the spatial distribution of active suspensions.

Microscale patchiness in the distribution of microorganisms has a profound effect on the ecology of aquatic environments and, cumulatively, may impact biogeochemical cycling at the global scale [1]. Field observations have revealed that the centimeter-scale distribution of motile species of phytoplankton is often considerably more patchy than that of nonmotile species [2–4]. Motility confers phytoplankton the ability to shuttle between well-lit waters near the surface during the day and pools of nutrient resources that reside deeper in the water column at night. This vertical migration is guided by a stabilizing torque, arising, for example, from bottom heaviness, which tends to keep a cell's swimming direction oriented upwards, and is opposed by hydrodynamic shear, which exerts a viscous torque on cells that tends to overturn them. When the swimming direction results from the competition between the cell's stabilizing torque and the shear-induced viscous torque, the organism is said to be gyrotactic [5]. Like other forms of directed motility, such as phototaxis [6,7] and chemotaxis [8,9], gyrotaxis can profoundly affect the spatial distribution of swimming plankton. In laminar flows, it produces remarkable beamlike accumulations in downwelling pipe flows [10] and concentrated layer accumulations in horizontal shear flows [11]. In turbulence, gyrotaxis generates intense microscale clustering at the Kolmogorov scale [12].

Previous models of gyrotaxis [5,11–16] have assumed that the stabilizing torque tends to align the cell opposite to the direction of gravity. In intense turbulent flows, however, fluid acceleration can locally exceed gravitational acceleration [17], and turbulence may thus change the typical orientation of phytoplankton relative to gravity, and with it the macroscopic spatial distribution of a population. In this Letter we use a combination of experiments and modeling to investigate the effect of fluid acceleration on the distribution of plankton swimming in turbulent flows.

We begin with an illustrative experiment by using a rotating, vertical cylinder as a simple proxy for a turbulent vortex. The cylinder is filled with a suspension of *Chlamydomonas augustae*, which, in a quiescent fluid, migrate upwards against gravity [18]. Rotation of the cylinder drives an accumulation of motile cells at the center of the cylinder, whereas dead cells remain uniformly distributed [Figs. 1(a) and 1(b)]. The classic model of gyrotactic motility [5], which does not include the effect of fluid acceleration on cell orientation, cannot account for this simple observation. A generalized model, which includes the effect of fluid acceleration, predicts temporal evolution of the swimming direction **p** (where $|\mathbf{p}| = 1$) and position X as

$$\frac{d\mathbf{p}}{dt} = -\frac{1}{2v_o}[\mathbf{A} - (\mathbf{A} \cdot \mathbf{p})\mathbf{p}] + \frac{1}{2}\boldsymbol{\omega} \times \mathbf{p}, \qquad (1)$$

$$\frac{d\mathbf{X}}{dt} = \boldsymbol{u} + v_C\mathbf{p}, \qquad (2)$$

where $\mathbf{A}$ is the total acceleration experienced by the cell [19], v_0 is the characteristic speed with which a perturbed cell reorients to the direction opposite to $\mathbf{A}$, $\boldsymbol{\omega} = \boldsymbol{\nabla} \times \boldsymbol{u}$ is
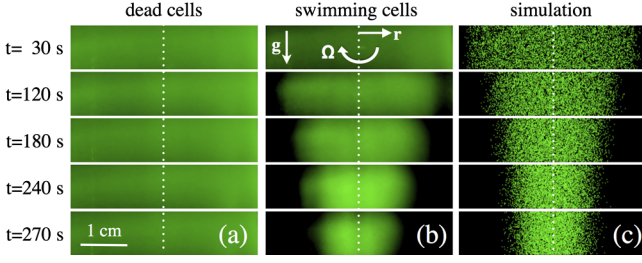
FIG. 1 (color online). Spatial distribution of gyrotactic swimmers in a rotating cylindrical vessel (radius 2 cm, volume 50 ml, rotation rate 5 Hz), obtained for (a) cells killed with 8% v/v ethanol, (b) swimming cells, and (c) simulated cells. The white dashed line denotes the axis of rotation and time is measured since the onset of the cylinder's rotation. (a),(b) A culture of *C. augustae* ($\sim 10^5$ cells/ml) illuminated with a green laser (50 mW) sheet. Brightness increases with cell concentration. (c) 10^4 synthetic swimmers, whose positions were obtained by integrating Eqs. (1) and (2) with flow velocity $\boldsymbol{u} = (-\Omega y, \Omega x, 0)$, with $\Omega = 10\pi$ rad s^{-1} and cell parameters $v_C = 100\ \mu$m s^{-1}, $B = v_o/g = 5$ s, and rotational diffusivity $D_r = 0.067$ rad^2 s^{-1}, closely approximating previous estimates for *C. augustae* [18].

the fluid vorticity at the cell location. For a bottom-heavy spherical cell $v_o = 3\nu/h$, where h is the distance from its center of mass to its geometric center and ν is the kinematic viscosity of the fluid. The cell velocity is the superposition of the fluid velocity at the cell location $\boldsymbol{u}$, and the swimming velocity $v_C\mathbf{p}$, where v_C is assumed to be constant. We assume that cells are neutrally buoyant, do not impact the flow, and, owing to their small size ($\sim 10\ \mu$m), can be modeled as point particles.

In the classic formulation [5,10] $\boldsymbol{A} = \boldsymbol{g} = -g\hat{\boldsymbol{z}}$ in Eq. (1) such that a cell's stabilizing torque aligns motility against gravity. This model cannot reproduce the accumulation observed in our experiments, because for solid-body rotation at angular velocity Ω, one has $\boldsymbol{\omega} = 2\Omega\hat{\boldsymbol{z}}$ and Eq. (1) predicts that (after a characteristic orientation time $B = v_o/g$) swimming becomes oriented along the vertical, $\mathbf{p} \to \hat{\boldsymbol{z}}$, maintaining the uniform initial distribution. Instead, if one accounts for the acceleration induced by the fluid measured in the reference frame of a cell, $\boldsymbol{A} = \boldsymbol{g} - \boldsymbol{a} = -g\hat{\boldsymbol{z}} + \Omega^2\boldsymbol{r}$, where $(\boldsymbol{r}, z)$ is the cylindrical coordinate system, the model predicts that a component of cell motility is directed radially inwards. Indeed, using the experimental configuration and the known motility parameters of *C. augustae*, the numerical integration of our model predicts cell distributions [Fig. 1(c)] in close agreement with those observed [Fig. 1(b)], suggesting that our generalization of the gyrotaxis equations captures the effect of fluid acceleration on cell motility. The trajectories of cells in Fig. 1(c) were calculated by adding an additional rotational diffusion term [18] to Eq. (1), which parametrizes the fluctuations in $\mathbf{p}$ arising from random cell behavior, stabilizing cell distribution at finite width about the axis of rotation at steady state.

The dynamics of this simple experiment, though bearing some resemblance to persistent small-scale vortices routinely found in turbulence [20], cannot capture the complexity of turbulent flows, which are inherently unsteady and incorporate multiple scales of fluid motion. To resolve the role of fluid acceleration in turbulent flows, we integrate the trajectories of cells within homogeneous, isotropic turbulence generated via direct numerical simulations (DNS) of the Navier-Stokes equations

$$\boldsymbol{a} \equiv \partial_t\boldsymbol{u} + \boldsymbol{u} \cdot \boldsymbol{\nabla}\boldsymbol{u} = -\boldsymbol{\nabla}p + \nu\nabla^2\boldsymbol{u} + \boldsymbol{f}, \qquad (3)$$

where $\boldsymbol{a}$ is the fluid acceleration, $\boldsymbol{u}$ is the incompressible fluid velocity ($\boldsymbol{\nabla} \cdot \boldsymbol{u} = 0$), and p is the pressure. The forcing $\boldsymbol{f}$ is a zero-mean, temporally uncorrelated Gaussian random field that injects kinetic energy at large scales at a rate ϵ, equal to the rate of energy dissipation at small scales $\epsilon = \nu\langle|\boldsymbol{\nabla}\boldsymbol{u}|^2\rangle_E$ (where $\langle[\ldots]\rangle_E = \int d^3x[\ldots]$ denotes the Eulerian average). We solve Eq. (3) on a triply periodic cubic domain containing $N^3 = 32^3 - 256^3$ grid points with a 2/3-dealiased pseudospectral method [21] to obtain flows with a Taylor Reynolds number of Re$_\lambda = \sqrt{15}u_{\text{rms}}^2/(\nu^{1/2}\epsilon^{1/2}) \approx 20$–100, where u_{rms} is the root-mean-square velocity fluctuation. Time stepping is performed with a second-order Runge-Kutta scheme explicitly accounting for the linear terms. The Kolmogorov length scale $\eta_K = (\nu^3/\epsilon)^{1/4}$ of the resulting flow is on the same order as our grid spacing ($k_{\max}\eta > 1.4$, where $k_{\max} = N/3$), ensuring that small-scale fluid motion is well resolved.

After the flow has reached statistical steady state, up to 3×10^6 cells with identical v_C and v_0 are initialized with random positions $\boldsymbol{X}$ and orientations $\mathbf{p}$. Cell trajectories are computed by integrating Eqs. (1) and (2) with fluid velocity, vorticity, and acceleration at the cell positions calculated by trilinear interpolation, which has been shown to accurately reproduce small-scale statistics in analogous simulations [22]. After cell distributions reach a statistical steady state, we collect data for a duration equivalent to several large-scale eddy turnover times to ensure statistical convergence. Rotational diffusion was not included to reduce the number of tunable parameters and because the decorrelation time scale due to stochastic motility (~ 15 s) is typically longer than the Kolmogorov time scale of moderately intense turbulence (e.g., $\tau_K = (\nu/\epsilon)^{1/2} \approx 1$ s for $\epsilon = 10^{-6}$ m^2 s^{-3}).

Two dimensionless parameters characterize cell motility in turbulent flow. The swimming number $\Phi = v_C/v_K$ quantifies the swimming speed relative to the Kolmogorov velocity $v_K = (\nu\epsilon)^{1/4}$. The stability number $\Psi_g = \omega_{\text{rms}}v_o/g$ measures the strength of the viscous torque exerted by fluid vorticity relative to the stabilizing torque, where g is taken as the characteristic acceleration scale. While, in general, cells are subjected to both gravitational and fluid acceleration, such that $\boldsymbol{A} = \boldsymbol{g} - \boldsymbol{a}$, we distinguish

two limits. The first limit $A = g$ considers only the influence of gravity on cell reorientation: a recent study found that cells in this regime form clusters in regions of downwelling flow [12]. The second limit $A = -a$ isolates the effect of fluid acceleration and requires defining a second stability number (because gravity can no longer be taken as the characteristic acceleration scale) $\Psi_a = \omega_{\mathrm{rms}} v_o / a_{\mathrm{rms}}$, where a_{rms} is the root-mean-square acceleration fluctuation. In this limit we find that cells aggregate in regions of high vorticity (Fig. 2), revealing that fluid acceleration is responsible for a second, fundamentally distinct mechanism that drives clusters of gyrotactic cells in turbulent flow.

Regardless of whether gravitational or fluid acceleration dominates, the "unmixing" of gyrotactic swimmers by turbulence can be explained by analyzing the contraction of the cells' phase space, defined by cell position and swimming orientation. Equations (1) and (2) define a dissipative dynamical system in the $(X, \mathbf{p})$ phase space of dimension $2d - 1$, and cells inhabit a three-dimensional volume such that $d = 3$. One can show the $(X, \mathbf{p})$ phase space contracts at a rate

$$\Gamma = \sum_{i=1}^{d} \left(\frac{\partial \dot{X}_i}{\partial X_i} + \frac{\partial \dot{p}_i}{\partial p_i} \right) = \frac{d-1}{2v_o} A \cdot \mathbf{p}. \quad (4)$$

Because the stabilizing torque of gyrotactic swimmers reorients $\mathbf{p}$ towards $-A$, we expect $A \cdot \mathbf{p}$ and, consequently, Γ to be negative on average, indicating that trajectories will collapse on a fractal attractor in phase space. If the fractal dimension of such an attractor is less than d, its projection onto the physical space will correspond to clusters with the same fractal dimension. A similar phenomenon occurs for inertial particles, where the contraction of the phase space, defined by particle position and velocity, leads to fractal
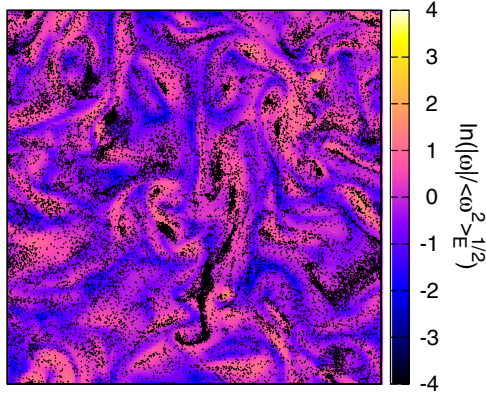
clustering [23,24]. In our case, both a nonzero swimming velocity and a nonzero stabilizing torque are required for clusters to form, as $\Gamma \to 0$ for both $\Phi \to 0$ and $\Psi_{g,a} \to \infty$; i.e., both nonmotile cells and motile cells without directional bias are predicted to remain randomly distributed.

To quantify fractal clustering, we measured the correlation dimension D_2, defined as the scaling exponent of the probability of finding two cells with a separation distance less than r: $P_2(|X_1 - X_2| < r) \propto r^{D_2}$ as $r \to 0$ [25]. $D_2 = d$ denotes randomly distributed cells, whereas $D_2 < d$ indicates fractal patchiness, with smaller D_2 corresponding to more clustered distributions and increased probability of finding pairs of swimmers at close separation. Figure 3 shows D_2 as a function of Ψ_g at different Re_λ. When compared with the case in which the local fluid acceleration is neglected [$\mathbf{A} = \mathbf{g}$ in Eq. (1); open circles in Fig. 3], these results demonstrate that fluid acceleration enhances clustering (smaller D_2). These findings are further supported by measurements of the generalized fractal dimension D_q, which quantifies the scaling behavior of the probability of finding q particles within a small separation r [25]. The nontrivial dependence on q, $D_q \neq D_2$, observed in Fig. 3 (inset) indicates that the dynamical attractor is multifractal [25].

To formalize the relative contributions of fluid and gravitational acceleration, it is useful to recast our simulations with different Re_λ in terms of the ratio $\alpha = a_{\mathrm{rms}}/g$.
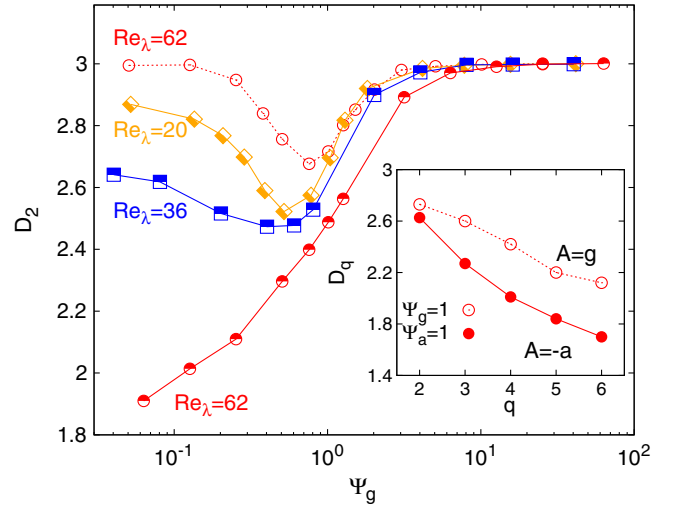
FIG. 2 (color online). Slice of a 3D turbulent flow, at $\mathrm{Re}_\lambda = 62$, showing cell clustering (black dots) in high vorticity regions when the stabilizing torque aligns them with the local fluid acceleration [$A = -a$ in Eq. (1)], $\Psi_a = 1.5$ and $\Phi = 1$. Shading shows the magnitude of the fluid vorticity relative to the Eulerian average.

FIG. 3 (color online). Correlation dimension D_2 versus stability number Ψ_g for increasing Re_λ (and ratio $\alpha = g/a_{\mathrm{rms}}$) at fixed dimensionless swimming speed $\Phi = 1/3$. Semifilled symbols refer to the complete model with $A = g - a$ in Eq. (1) with $\mathrm{Re}_\lambda = 20$ ($\alpha = 0.34$) (orange diamonds), $\mathrm{Re}_\lambda = 36$ ($\alpha = 0.50$) (blue squares), and $\mathrm{Re}_\lambda = 62$ ($\alpha = 0.84$) (red circles). Open (red) circles denote the case where cell orientation is determined by gravity only, $A = g$ at $\mathrm{Re}_\lambda = 62$. Inset: the generalized dimension D_q as a function of q, at $\mathrm{Re}_\lambda = 62$ when only gravitational ($A = g$, open circles) or fluid acceleration ($A = -a$, filled circles) is considered.

We start by briefly summarizing the case $\alpha = 0$, when fluid acceleration is negligible and $A = g$, analyzed in Ref. [12]. In this limit, D_2 is insensitive to Re_λ and reaches a minimum (denoting maximal clustering) at stability numbers $\Psi_g = O(1)$ (Fig. 3, open circles), intermediate between strictly upward motility ($\Psi_g \ll 1$) and isotropic motility ($\Psi_g \gg 1$). Moreover, one can theoretically predict that cells preferentially concentrate in downwelling regions (i.e., where $u_z < 0$). Assuming $\Psi_g \ll 1$ allows Eq. (1) to be expanded to first order in Ψ_g, such that cells behave as tracers advected by a velocity field $\dot{X} = v(X, t)$ that is weakly compressible. One can show that $\nabla \cdot v = -\Phi\Psi_g \nabla^2 u_z$, which predicts that cells preferentially accumulate where $\nabla^2 u_z > 0$, which corresponds to local downwelling flow $u_z < 0$, because $\langle u_z \nabla^2 u_z \rangle_E = -\epsilon/(3\nu) < 0$ in isotropic turbulence (see Ref. [12] for details). This argument also correctly predicts that compressibility increases, enhancing clustering, with the swimming speed Φ (for small Ψ_g) and vanishes at $\Psi_g = 0$. At large Ψ_g, vorticity overturning dominates and cells swim in random orientations. The competition between these two mechanisms explains the minimum in D_2.

As α increases from zero, the minimum D_2 becomes progressively smaller, indicating more intense clustering, and shifts towards smaller values of Ψ_g, eventually disappearing as α increases further (Fig. 3, semifilled symbols). These results indicate that fluid acceleration substantially enhances cell clustering for $\Psi_g \ll 1$ and this effect increases with the turbulence intensity (larger Re_λ).

To understand how fluid acceleration drives clustering, we performed simulations where $A = -a$. In this limit, results for different Re_λ collapse when plotted as a function of Ψ_a, with a weak residual dependence on Re_λ [Fig. 4(a)], confirming that cell stability is the key parameter controlling clustering. In addition, cells cluster more strongly as cell stability ($1/\Psi_a$) and swimming speed (Φ) increase [Fig. 4(a)], corroborating our findings with the full model (Fig. 3). To rationalize these observations with a theoretical model, we assume $\Psi_a \ll 1$ such that a cell's stabilizing torque dominates the torque arising from fluid vorticity. In this limit $\mathbf{p}$ instantaneously aligns with the local direction of the fluid acceleration $\hat{a} = a/a$, so that cells move with velocity $v \approx u + \Phi\hat{a}$, which is valid to the first order in Ψ_a. While the fluid velocity u is incompressible, v is not, because $\nabla \cdot v \approx \Phi\nabla \cdot \hat{a} \neq 0$. Moreover, DNS data show that the sign of $\nabla \cdot a$ is strongly correlated to that of $\nabla \cdot \hat{a}$. Therefore, when $A = -a$, gyrotactic cells are expected to accumulate in regions where $\nabla \cdot a < 0$. These regions correspond to zones of high fluid vorticity because taking the divergence of Eq. (3) yields $\nabla \cdot a = \sum_{ij}(\hat{S}_{ij}^2 - \hat{\Omega}_{ij}^2)$, with $\hat{S}_{ij} = (\partial_j u_i + \partial_i u_j)/2$ and $\hat{\Omega}_{ij} = (\partial_j u_i - \partial_i u_j)/2$ being the rate of strain tensor and vorticity tensor, respectively. This mechanism bears some resemblance to the clustering of nonmotile, light inertial particles (e.g., bubbles in water) [26,27], which, in the limit of small inertia,
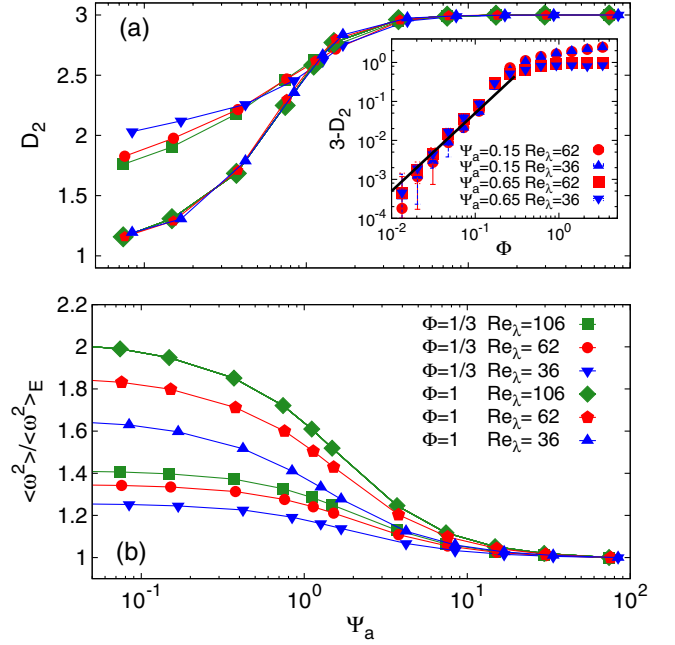

FIG. 4 (color online). Results of simulations for the model with fluid acceleration only, $A = -a$. (a) Correlation dimension and (b) square vorticity averaged over particle positions $\langle\omega^2\rangle$ and normalized by the Eulerian value $\langle\omega^2\rangle_E$ as a function of the stability number Ψ_a for different values of Re_λ and nondimensional swimming speeds Φ. Inset of panel (a): the codimension $3 - D_2$ as a function of Φ at different Re_λ and Ψ_a in log-log plot. The straight line shows the theoretical prediction $3 - D_2 \propto \Phi^2$.

also move relative to the flow in a direction aligned with the local fluid acceleration [26–28]. However, there are also important differences: the speed of light particles relative to the fluid is proportional to the magnitude of acceleration and to the parameter controlling inertia (the Stokes number, assumed to be small in this approximation), while the speed of gyrotactic cells relative to the fluid is constant and independent of Ψ_a. The accumulation of gyrotactic cells in high vorticity regions is demonstrated qualitatively in Fig. 2 and is quantified in Fig. 4(b), which shows that the square vorticity averaged over all cell positions is considerably enhanced over the fluid background value, and increases with both Re_λ and Φ. General dynamical systems considerations [29,30] predict that, in weakly compressible flows, the codimension $3 - D_2$ is proportional to the square of the intensity of the divergence of the velocity field. Therefore, for stable cells ($\Psi_a \ll 1$), in the limit of small Φ, one predicts $3 - D_2 \propto \Phi^2$, which is in excellent agreement with DNS data [Fig. 4(a) inset].

Our results indicate that distribution of gyrotactic swimmers becomes significantly more clustered when fluid acceleration is on the same order as gravitational acceleration. However, turbulence in natural environments is often too weak to reach this regime. For example, the energy dissipation rate in the ocean rarely exceeds

$\epsilon \sim 10^{-4}$ m^2/s^3, corresponding to $a_{\text{rms}} \simeq (\epsilon^3/\nu)^{1/4} \simeq$ 0.1 m/s$^2 \ll g$. Thus, under most marine conditions we expect that cell distributions can be well characterized assuming reorientation occurs due to gravitational acceleration alone, $A = g$ [12]. We note, however, that nonhomogeneous conditions, such as solid boundaries, can generate intense vorticity at moderate Reynolds numbers and thus may drive fluid acceleration induced cell clustering in the bottom boundary layer. A similar phenomenon may occur in laboratory studies of plankton, which often employ turbulent dissipation rates much higher than found in the ocean's upper mixed layer [31]. Another prominent environment with intense turbulence occurs in engineered biofuel production facilities, where turbulent mixing is used to prevent self-shading and biofouling [32,33]. The clustering mechanism demonstrated here likely dramatically increases cell-cell encounter rates and, therefore, may lead to undesirable cell aggregates that enhance sedimentation. We finally remark that the effective compressibility generated by gyrotactic motility in turbulence may have far reaching implications for population dynamics and genetics [34,35] of these tiny inhabitants of the oceans.

---

*Corresponding author.
massimo.cencini@cnr.it

[1] F. Azam and F. Malfatti, Nat. Rev. Microbiol. **5**, 782 (2007).
[2] E. Malkiel, O. Alquaddoomi, and J. Katz, Meas. Sci. Technol. **10**, 1142 (1999).
[3] S. M. Gallager, H. Yamazaki, and C. S. Davis, Mar. Ecol. Prog. Ser. **267**, 27 (2004).
[4] L. T. Mouritsen and K. Richardson, J. Plankton Res. **25**, 783 (2003).
[5] T. J. Pedley and J. O. Kessler, Proc. R. Soc. B **231**, 47 (1987); , Annu. Rev. Fluid Mech. **24**, 313 (1992).
[6] C. Torney and Z. Neufeld, Phys. Rev. Lett. **101**, 078105 (2008).
[7] X. Garcia, S. Rafaï, and P. Peyla, Phys. Rev. Lett. **110**, 138106 (2013).
[8] E. O. Budrene and H. C. Berg, Nature (London) **349**, 630 (1991).
[9] J. R. Seymour, Marcos, and R. Stocker, Am. Nat. **173**, E15 (2009).
[10] J. O. Kessler, Nature (London) **313**, 218 (1985).
[11] W. M. Durham, J. O. Kessler, and R. Stocker, Science **323**, 1067 (2009).
[12] W. M. Durham, E. Climent, M. Barry, F. De Lillo, G. Boffetta, M. Cencini, and R. Stocker, Nat. Commun. **4**, 2148 (2013).
[13] N. A. Hill and M. A. Bees, Phys. Fluids **14**, 2598 (2002).
[14] G. J. Thorn and R. N. Bearon, Phys. Fluids **22**, 041902 (2010).
[15] W. M. Durham, E. Climent, and R. Stocker, Phys. Rev. Lett. **106**, 238102 (2011).
[16] O. A. Croze, G. Sardina, M. Ahmed, M. A. Bees, and L. Brandt, J. R. Soc. Interface **10**, 20121041 (2013).
[17] A. La Porta, G. Voth, A. Crawford, J. Alexander, and E. Bodenschatz, Nature (London) **409**, 1017 (2001).
[18] C. Williams and M. Bees, J. Fluid Mech. **678**, 41 (2011).
[19] F. De Lillo, M. Cencini, G. Boffetta, and F. Santamaria, J. Turbul. **14**, 24 (2013).
[20] L. Biferale, G. Boffetta, A. Celani, A. Lanotte, and F. Toschi, Phys. Fluids **17**, 021701 (2005).
[21] C. Canuto, M. Hussaini, A. Quarteroni, and T. Zang, *Spectral Methods in Fluid Dynamics* (Springer–Verlag, Berlin, 1988).
[22] L. Biferale, G. Boffetta, A. Celani, B. J. Devenish, A. Lanotte, and F. Toschi, Phys. Rev. Lett. **93**, 064502 (2004).
[23] J. Bec, J. Fluid Mech. **528**, 255 (2005).
[24] J. Bec, L. Biferale, M. Cencini, A. Lanotte, S. Musacchio, and F. Toschi, Phys. Rev. Lett. **98**, 084502 (2007).
[25] G. Paladin and A. Vulpiani, Phys. Rep. **156**, 147 (1987).
[26] E. Balkovsky, G. Falkovich, and A. Fouxon, Phys. Rev. Lett. **86**, 2790 (2001).
[27] E. Calzavarini, M. Cencini, D. Lohse, and F. Toschi, Phys. Rev. Lett. **101**, 084504 (2008).
[28] M. Maxey, J. Fluid Mech. **174**, 441 (1987).
[29] G. Falkovich, A. Fouxon, and M. Stepanov, Nature (London) **419**, 151 (2002).
[30] I. Fouxon, Phys. Rev. Lett. **108**, 134502 (2012).
[31] F. Peters and J. M. Redondo, Sci. Mar. **61**, 205 (1997).
[32] Y. Chisti, Biotechnology advances **25**, 294 (2007).
[33] M. A. Bees and O. A. Croze, Biofuels **5**, 53 (2014).
[34] S. Pigolotti, R. Benzi, M. H. Jensen, and D. R. Nelson, Phys. Rev. Lett. **108**, 128102 (2012).
[35] R. Benzi, M. H. Jensen, D. R. Nelson, P. Perlekar, S. Pigolotti, and F. Toschi, Eur. Phys. J. Spec. Top. **204**, 57 (2012).